Moroccan Journal of Chemistry
ISSN: 2351-812X
http://revues.imist.ma/?journal=morjchem&page=login
El Aoufir & al. / Mor. J. Chem. 5 N°4 (2017) 545-559

Triazole derivative as new and effective corrosion inhibitor for carbon steel in hydrochloric acid: Electrochemical and quantum chemical studies

Y. El aoufir[1,2], Y. El Bakri[3], Y. Kerroum[2], H. Lgaz[1,3], A. Harmaoui[4], A. Chetouani[5], J. Sebhaoui[3], R. Salghi[3*], Y. Ramli[6], A. Guenbour[2], E.M. Essassi[3], H. Oudda[1]

[1] *Laboratory of Separation Processes, Université Ibn Tofail, Faculté des Sciences, Kenitra, Morocco.*

[2] *Laboratory of Nanotechnology, Materials & the Environment University Mohammed V, Faculté des Sciences, Rabat, Morocco.*

[3]*Laboratory of Applied Chemistry and Environment, ENSA, Ibn Zohr University, PO Box 1136, 80000 Agadir, Morocco*

[4] *Laboratoire de Chimie Organique Hétérocyclique, Université Mohammed V, Faculté des Sciences, Rabat, Morocco*

[5]*Laboratoire de Chimie Appliquée et environnement (LCAE-URAC18), Faculté des Sciences, 60000 Oujda, Morocco.*

[6]*Medicinal Chemistry Laboratory, Faculty of Medicine and Pharmacy, Mohammed V University in Rabat, 10170 Rabat, Morocco.*

* *Corresponding author:*
r.salghi@uiz.ac.ma

Received 25 Jan 2017,
Revised 17 July 2017,
Accepted 28 July 2017

Abstract

The corrosion inhibition properties of triazole derivative via 3,4-diamino-1,2,4-triazole (TRD) were investigated by the electrochemical impedance spectroscopy (EIS) and potentiodynamic polarization methods. The results of electrochemical research revealed that the TRD was adsorbed on the metal surface by adsorption mechanism and behave as mixed type inhibitor. The Among TRD exhibited maximum efficiency of 90% at 10-3M. The inhibition mechanism was analyzed by the potential of zero charge (Epzc) measurement at the solution/metal interface. The adsorption behaviour of the 3,4-diamino-1,2,4-triazole on Fe (110) surface was investigated by Monte Carlo simulations to verify their corrosion inhibition efficacies.

Keywords: *, hydrochloric acid, EIS, PDP, DFT, Molecular Dynamic simulations.*

1. Introduction

Carbon steel have been extensively used as a material because it is characterized by low cost, easy to weld, very hard in the different applications, such as automobile chassis, motorcycle frames, building, and most cookware. But it doesn't have much resistance to corrosion in corrosive media like solutions containing halide ions that increase the metal dissolutions [1-5]. In the industrial process like descaling and pickling the carbon steel expose to aggressive acids such as sulphuric and hydrochloric acids causes deeply degradation of material [6, 7]. Most well-known methods used to protect the material are the use corrosion inhibitors. They stay the most practical and cost effective method. The organic compounds are largely applied in hydrochloric acid solutions as effective corrosions inhibitors [8]. The existence of sulfur, oxygen, and nitrogen atoms is reported to be responsible to this efficiency in many researches [9-15]. As one of the majorities often used carbon steel inhibitors, triazole derivatives have been studied, especially in the hydrochloric acid solution [16-18]. They were demonstrated an efficient corrosion inhibition. Previously, Investigation of 1,2, 4-Triazoles as corrosion inhibitor for steel in hydrochloric acid medium have been reported as potential corrosion inhibitors [6-33]. In this paper we prolong our studies on 3,4-diamino-1,2,4-triazole as corrosion inhibitor of steel in hydrochloric acid medium. The properties of the inhibition were examined profoundly via polarization, electrochemical impedance spectroscopy (EIS), Potential zero charge (pzc), isotherm calculations. The experimental results were correlated with quantum chemical calculations.

2. Materials and methods

2.1. Synthesis of corrosion inhibitor

Synthesis of 3,4-diamino-1,2,4-triazole: A solution of 0.03 mol of diamino guanidine hydrobromide resumed by 6 cm^3 of dioxane and 2 cm^3 of formic acid and then refluxed for 2 hours.

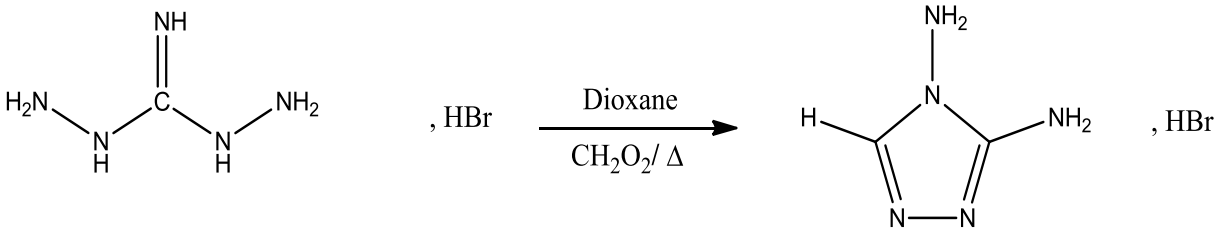

The compound was characterized by N.M.R. ^{1}H-NMR (DMSO-d6) (d ppm): 6.99(s,2H,NH_2), 5.77(s,2H,NH_2), 8.29(s,1H;CH). ^{13}C-NMR(DMSO-d6) (d ppm): 142.5(C=N), 155.8(C=N).

Table 1. IUPAC name and molecular structure

Name of inhibitor	Chemical structure
3,4-diamino-1,2,4-triazole (TRD)	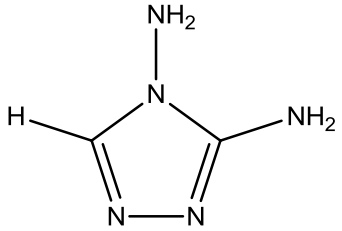

2.2. *Specimens*

Corrosion inhibition tests by electrochemical measurements in 1M HCl were performed using coupons prepared from carbon steel having the composition: 0.370 % C, 0.230 % Si, 0.680 % Mn, 0.016 % S, 0.077 % Cr, 0.011 % Ti, 0.059 % Ni, 0.009 % Co, 0.160 % Cu and the remainder iron (Fe). For electrochemical studies, specimens with an exposed

area of 1 cm^2 were used. The carbon steel specimens were polished with increasing grades of emery papers (100, 220, 360, 400, 600 and 1200 grit size), then degreased with acetone and washed with deionized water. Finally, the specimens were dried at room temperature.

2.3. *Solutions*

The aggressive solution was prepared by dilution of analytical grade HCl (37%) with distilled deionized water. The concentrations of the studied inhibitors ranged from 10^{-3}M to 10^{-6}M and the volume of test solution used for electrochemical studies was 50 ml. The test solutions were recently prepared before each experiment by adding inhibitor TRD directly to the corrosive solution.

2.4. *Electrochemical measurements*

The electrochemical methods were carried out by the means of a Volta lab (Radiometer PGZ 100) potentiostat and controlled by corrosion analysis software (Voltamaster 4). The corrosion behaviour of the CS specimens was studied in a 1M HCl solution using EIS, and potential polarization curves in the inhibitor-free and presence of inhibitor solutions. Corrosion tests were performed in a three-electrode cell. An Ag/ AgCl electrode was used as a reference electrode along with a platinum sheet (with a $1cm^2$ surface area) as a counter electrode. The CS was immersed in the test solution for 30 min to set up the balanced state E_{ocp}. The EIS measurements were immediately performed under measured E_{ocp}, start-up frequency ranges of 100 kHz to 10 mHz and an amplitude of 10mV (peak to peak). In the entire experiment, the Nyquist diagrams were fitted using the EcLab program. To get the corrosion parameters, the cathodic and anodic polarization tests were also performed starting from E_{ocp}, using scan rate of 2 mV s^{-1} after reaching a steady state E_{ocp}.

2.5. *Measurement of potential of zero charge*

In order to determine the potentiel of zero charge (E_{pzc}), the EIS measurements were performed in the 1M HCl solutions in the presence of 10^{-3}M TRD at different potentials with an AC amplitude of 10 mV. A plot of C_{dl} against the applied potentiels was obtained to determine the E_{pzc}. The excess surface charge of CS was determined in the test solution by the location of the E_{ocp} with respect to the E_{pzc}.

2.6. *DFT method detail*

E_{HOMO} (highest occupied molecular orbital energy), E_{LUMO} (lowest unoccupied molecular orbital energy) and Fukui indices calculations were performed using $DMol^3$ module in Materials Studio version 6.0[36]. These calculations employed an *ab initio*, gradient-corrected functional (GGA) method with a double numeric plus polarization (DNP) basis set and a Becke One Parameter (BOP) functional. It is well-known that the phenomena of electrochemical corrosion appear in aqueous phase. $DMol^3$ includes certain COSMO controls, which allow for the treatment of solvation effects[37,38]. The absolute electronegativity (χ) and global hardness (η) of the inhibitors molecule are approximated as follows[39,40]:

$$\chi = \frac{IP+EA}{2} \quad (1)$$

$$\eta = \frac{IP-EA}{2} \quad (2)$$

where: $I = -E_{HOMO}$ and $A = -E_{LUMO}$

Thus the fraction of electrons transferred from the inhibitor to metallic surface, ΔN, is given by[41]:

$$\Delta N = \frac{\emptyset - \chi_{inh}}{2(\eta_{Fe} + \eta_{inh})} \quad (3)$$

The theoretical values of $\emptyset$ (4.06 eV mol^{-1}) and of η_{Fe} (0 eV mol^{-1}) are used to calculate ΔN[40,42].

2.7. *Monte Carlo simulation study*

The Monte Carlo (MC) search was adopted to compute the low configuration adsorption energy of the interactions of the TRD on a clean iron surface. The Monte Carlo (MC) simulation was carried out using Materials Studio 6.0 software (Accelrys, Inc.)[36]. The Fe crystal was cleaved along the (1 1 0) plane, it is the most stable surface as reported in the literature. Then, the Fe (1 1 0) plane was enlarged to (12x12) supercell to provide a large surface for the interaction of the inhibitor. The simulation of the interaction between TRD and the Fe (1 1 0) surface was carried out in a simulation box (19.85 × 19.85 × 38.11 Å) with periodic boundary conditions, which modeled a representative part of the interface devoid of any arbitrary boundary effects. After that, a vacuum slab with 30 Å thickness was built above the Fe (110) plane. All simulations were implemented with the COMPASS force field to optimize the structures of all components of the system of interest. More simulation details on the methodology of Monte Carlo simulations can be found in previous publications[43–45].

3. Results and Discussions

3.1. Potentiodynamic polarization measurements

Potentiodynamic polarization measurements allow determining the corrosion inhibition mechanism of metals. Thus, potentiodynamic polarization curves are seen in Fig. 1 for inhibited and uninhibited solutions. As would be expected from Fig. 1, inhibitor molecules evidently inhibit for both anodic and cathodic reactions which was indicated by diminution of current densities with augmentation of concentration of TRD. As known, cathodic and anodic regions correspond to hydrogen evolution and iron dissolution reactions under the experimental conditions, respectively. Considering the addition of TRD, both the current densities of cathodic and anodic reactions reduce effectively and this reduction becomes more pronounced with increasing TRD concentration, meaning that this molecule could be classified as a mixed-type inhibitor. From these results TRD is observed to prevent CS corrosion by blocking the reaction sites effectively. The optimum corrosion inhibition efficiencies are found to be 87% at 10^{-3} M of inhibitor.

Polarization curves of the carbon steel in 1M HCl solutions without and with addition of different concentrations of TRD are shown in Fig. 1. The anodic and cathodic current–potential curves are extrapolated up to their intersection at a point where corrosion current density (I_{corr}) and corrosion potential (E_{corr}) are obtained [46]. Table 2 shows the electrochemical parameters (I_{corr}, E_{corr}, and β_c) obtained from Tafel plots for the steel electrode in 1 M HCl solution without and with different concentrations of the TRD. The I_{corr} values were used to calculate the inhibition efficiency, E (%) (Listed in Table 3), using the following equation [47], where, I°_{corr} and I^{i}_{corr} are the corrosion current density in absence and presence of inhibitor, respectively.

$$\eta_{Tafel}\% = \frac{I^{\circ}_{corr} - R^{i}_{corr}}{R^{\circ}_{corr}} \times 100 \qquad (4)$$

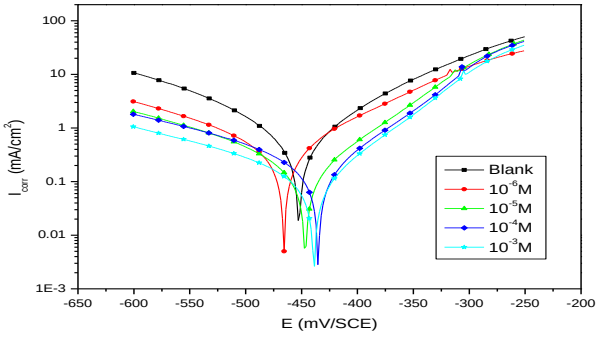

Figure 1. Potentiodynamic polarization curves for carbon steel at 303 K in 1M HCl solution in the absence and the presence of TRD at various concentrations.

Table 2. Kinetic parameters calculated from PDP measurements after 30min of immersion in 1M HCl solution with and without inhibitor concentrations of TRD at 303K.

Inhibitor	Concentration (M)	E_{corr} (mV/SCE)	I_{corr} (mA cm^{-2})	β_a (mV dec^{-1})	$-\beta_c$ (mV dec^{-1})	η (%)
Blank	1	-452.1	0.858	113.7	131.2	-
TRD	10^{-6}	-465.8	0.351	99.6	134.8	59
	10^{-5}	-445.6	0.173	77.0	143.2	79
	10^{-4}	-434.9	0.173	74.9	157.6	80
	10^{-3}	-438.8	0.110	71.4	161.6	87

3.2. AC impedance study

The corrosion inhibition property of 3, 4-diamino-1,2,4-triazole on carbon steel was examined by electrochemical impedance spectroscopy (EIS). This method is a good technique in investigating corrosion inhibition processes. It provides information on both the resistive and capacitive behavior at interface and makes it possible to evaluate the performance of the tested compounds as possible inhibitor against metals corrosion. Fig. 1 show the Nyquist plots of carbon steel obtained at open circuit potential in 1M HCl solution without and whit different concentrations of TRD. The Nyquist diagram shows in Fig.2 that the impedance diagrams are larger than in the blank solution, when the TRD are added to the corrosive solution. The size of the impedance diagram increases whit augmentation of concentration and consequently the protection efficiency increases. This observation can be explain by adsorption of inhibitor molecule on the metal surface [48]. Fig. 2 showed one capacitive loop as represented by slightly depressed semi-circle for the inhibitor. This capacitive loop revealed that corrosion of the carbon steel in 1M HCl solution is mainly controlled by the charge transfer process and the formation of a protective layer on the metal surface in the presence of inhibitor and inhomogeneity of the metal surface. Thence, constant phase element (CPE) is introduced in the circuit to get a more accurate fit [49–51]. The CPE impedance is defined by two values, Q and ω his described by the equation:

$$Z_{CPE} = Q^{-1}.(i\omega)^{-n} \qquad (5)$$

where Q is the CPE constant, ω is the angular frequency (in rad s^{-1}), $i^2 = -1$ is the imaginary number and n has the meaning of phase shift [52]. The factor n is an adjustable parameter that usually lies between 0.50 and 1.0 [53]. The CPE describes an ideal capacitor when $n = 1$. The impedance spectra were fitted by a simple Randles circuit (Fig. 2), which consists of charge transfer resistance (R_{ct}) connected in parallel to constant phase element for double layer (CPE), both in series with solution resistance (R_s). A constant phase element (CPE) is used instead of a pure capacitor to compensate for non-ideal capacitive response of the interface [54, 55]. All the impedance parameters such as charge transfer resistance (R_{ct}), double layer capacitances (C_{dl}), relaxation time constant (τ) and inhibition efficiency (η_Z) were listed in Table 3.

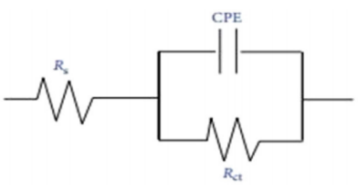

Figure 3. Suggest equivalent model for the studied system

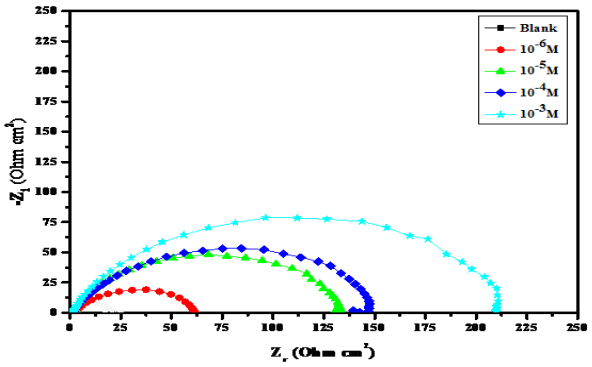

Figure 2. Nyquist plots for carbon steel at 303 K in 1M HCl in various concentrations of the studied inhibitor: TRD

Table 3. Electrochemical impedance spectroscopy measurements for carbon steel immersed in 1M HCl for 30 min in the absence and presence of different concentrations of the synthesized inhibitor.

	Conc (M)	R_s (Ω cm^2)	R_{ct} (Ω cm^2)	10^4Q (Ω^{-1}cm^{-2}s^{-n})	n	C_{dl} (μF cm^{-2})	τ (F Ω)	η (%)
Blank	1M	0.574 5	20.14	4.55	0.86	220.5	4.44E-3	-
TRD	10^{-6}	2.459	59.88	4.45	0.73	113.9	6.82E-3	66.36
	10^{-5}	0.991 4	134.2	1.94	0.79	73.68	9.89E-3	85
	10^{-4}	1.013	150.6	1.82	0.78	65.79	9.91E-3	86.66
	10^{-3}	1.399	212.5	1.2	0.82	54.27	1.15E-2	90.52

Inhibition efficiency is related to charge transfer resistance. The charge transfer resistance value (R_{ct}) is calculated from the difference in real impedance at lower and higher frequencies. On increasing concentration of the inhibitor, charge transfer resistance increases as the inhibitor forms an adsorbed layer on metal surface. This also results in the increase in diameter of the semicircle. Inhibition efficiency can be calculated by R_{ct} using the following formula:

$$\eta_Z\% = \frac{R^i_{ct} - R^\circ_{ct}}{R^i_{ct}} \times 100 \qquad (6)$$

where, R°_{ct} and R^i_{ct} are the charge transfer resistance in absence and in presence of inhibitor, respectively.

The relaxation time constant (τ) of charge-transfer process using the following equation [56]:

$$\tau = C_{dl} * R_{ct} \qquad (7)$$

Results of the present work showed that the values of R_{ct} and η increase with increase in TRD concentration, while the C_{dl} values tend to decrease (see the data presented in Table 3). This indicates a reduction in the steel corrosion rate and that this compound are acting as adsorption inhibitor. The double layer between the charged metal surface and the solution is considered as an electrical capacitor. Fig. 4 shows the diagrams of Bode and phase angle. They are recorded for carbon steel electrode immersed in 1M HCl in the absence and presence of various concentrations of inhibitor. A phase angle shift with the concentration rise of inhibitors was observed. The phase angle shift can be attribueted to the formation of the protective film on the steel surface, which changed the electrode interfacial structure [57]. At higher concentration, as the surface area occupied by Schiff bases is more the phase shift is also more. The tendency of the current which passes through capacitor can be explain by an increment in the value of impedance with increasing concentration of inhibitors.

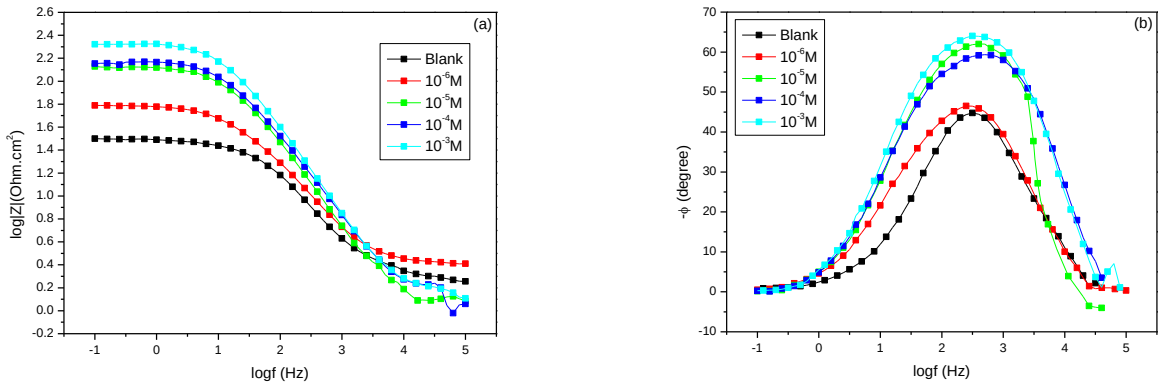

Figure 4. Bode (a) and phase angle (b) plots in the absence and presence of different concentrations of TRD.

3.3. Adsorption isotherm

The adsorption isotherm is considered among the most important subjects of corrosion, since it provides information about the nature of the interaction between the inhibitory molecule and the metal surface. As it also provides structural information on two layers in addition to the thermodynamic information. The adsorption may be chemisorption, physisorption or mixed type adsorption. Different isotherms were tested such us, Langmuir, Temkin, Frumkin and Freundlich in order to determine the nature of the adsorption of the inhibitor studied on the metal surface. However, the value of the regression coefficient (R^2) that gave the best fit is that of the Langmuir isotherm, because that is the value of R^2 closes to unity for this inhibitor. According to the Langmuir isotherm, the degree of surface coverage (θ) is related to the inhibitor concentration (C) by following relation [58]:

$$\frac{\theta}{1-\theta} = K_{ads} C_{inh} \qquad (8)$$

where K_{ads} is the equilibrium constant of the adsorption process, C is the molar concentration of TRD and θ is the degree of surface coverage of TRD at metallic surface. The values of surface coverage obtained at different concentrations of the TRD from PDP experiments were used to obtain the Langmuir adsorption isotherm plots (Fig. 5) which enabled the calculation of the values of K_{ads}. The K_{ads} related to the standard free energy of adsorption (ΔG^0_{ads}) by the following relation [59]:

$$\Delta G^{\circ}_{ads} = -RT\ln(55.5K_{ads}) \qquad (9)$$

Where R is the universal gas constant, T the absolute temperature and the value of 55.5 is the molar concentration of water in the solution.

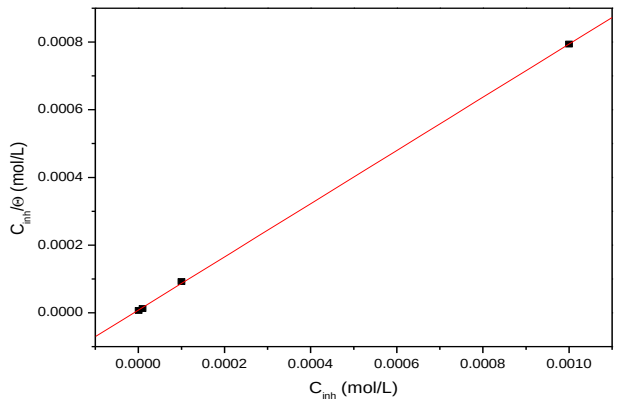

Figure 5. Langmuir adsorption isotherm plot for carbon steel in 1M HCl at different concentrations of the studied inhibitors.

The calculated values of K_{ads} and ΔG^0_{ads} are indicating in Table 4. High values of K_{ads} suggest that the adsorption of the TRD on carbon steel surface is easy and strong [60]. Previous, studies show that the value of ΔG^0_{ads} is more negative than −40 kJ mol^{-1} is consisted with charge sharing between metal and inhibitor molecule (chemisorption) [61, 62]. While the value of ΔG^0_{ads} is less negative than −20 kJ mol^{-1} is consisted with electrostatic interaction between charged inhibitor molecule and metallic surface (physisorption) [61, 62]. Results depicted in Table 4 showed that values of ΔG^0_{ads} in the present study at different temperatures vary from −39.70 kJ mol^{-1} suggesting that adsorption of the TRD on carbon steel surface is physisorption and chemisorption [63, 64]

Table 4. The values of K_{ads} and ΔG°_{ads} for carbon steel of TRD in 1M HCl at 303 K.

Inhibitors	K_{ads} (M^{-1})	$-\Delta G^\circ_{ads}$ (KJ.mol^{-1})	R^2
TRD	0.12603E6	39.70	0.99994

3.4. The potential of zero charge and the inhibition mechanism

The electrostatic interaction between the carbon steel and the inhibitor is used to determine the adsorption behaviour and the ability of inhibition by forming a protective film that possesses the organic inhibitors. The surface charge of the metal can be investigated by comparing the open circuit potentiel (E_{ocp}) with the potential of zero charge (E_{pzc}). A plot of the C_{dl} vs the applied potentials is exemplified in Fig. 6. The surface charge of carbon steel can be explored using the equation:

$$E_\Gamma = E_{ocp} - E_{pzc} \qquad (10)$$

where E_Γ is the rational corrosion potentiel [65,66]. As it is shown in Fig. 6, the curve appears parabolic in shape, with a minimum at 450 mV/SCE. This point is the E_{pzc} of the CS in 1M HCl solution containing 10^{-3}M of TRD [67]. The E_{ocp} of CS under the same conditions is -438 mV/SCE, which is more positive than the E_{pzc}, indicating a positively charged CS surface (Er = +12 mV/SCE). This result indicate that anions (Cl^- ions) in aqueous hydrochloric acid solution will be first to get adsorbed on the steel surface. After this, the steel surface will become negatively charged. Hence, the positively charged of TRD cationic forms will form an electrostatic bond with the Cl^- ions already adsorbed on steel surface [68].

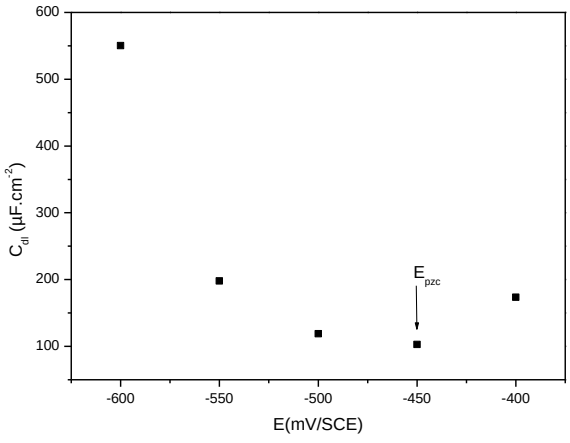

Figure 6. Plot of C_{dl} vs. applied electrode potential in 1 M HCl containing 10^{-3} M of TRD.

3.5. Effect of temperature

Several actions can occur on the surface of metal such as rapid burning, desorption of the inhibitor and the inhibitor itself may undergo decomposition, this is what, the effect of temperature on the metal-acid reaction inhibited is very

complex [64]. In order to evaluate the effect of temperature on the inhibition performance of TRD, potentiodynamic polarization potential experiments was performed in 1 M HCl without and with 10^{-3}M of inhibitor from 303 to 333 K (see figures 7a and 7b). It can be seen that the corrosion current density increases with temperature in the absence and presence of TRD. We also note that the inhibitor investigated have been inhibiting properties at all temperatures studied and the values of inhibition efficiency increase slightly even if the temperature rises (table 5). The inhibition efficiencies, calculated from ac impedance study, show the same trend as these obtained from polarization measurements. The inhibitor studied acts as an effective inhibitor in the temperature range between 303 and 333 K, because the corrosion current density for steel increases more rapidly with temperature in the solution without inhibitor. According to corresponding data in Table 5, some activation parameters of the corrosion process, the activation energy (E_a), the enthalpy of activation (ΔH_a) and the entropy of activation (ΔS_a) can be obtained by the Arrhenius formula and transition state equation, respectively [69]:

$$I_{corr} = Aexp\left(-\frac{E_a}{RT}\right) \qquad (11)$$

where E_a is the apparent activation corrosion energy, R is the universal gas constant and k is the Arrhenius pre-exponential constant. Taking the logarithm of the Arrhenius equation yields:

$$\mathrm{Ln}I_{corr} = \mathrm{Ln}A + \left(-\frac{E_a}{RT}\right) \qquad (12)$$

The Arrhenius plots of the logarithm of the current density versus 1/T for carbon teel in the HCl medium in presence and absence of 10^{-3} M of TRD is show in fig 8. Straight lines are obtained with a slope of (Ea/R). Activation parameters obtained from this graph are given in Table 6. The value of E_a found for TRD is inferior to that obtained for aggressive solution. The decrease in the apparent activation energy may be interpreted as chemical adsorption of inhibitor on steel surface [70]. An alternative formulation of Arrhenius equation is [71]:

$$I_{corr} = \frac{RT}{Nh}\exp\left(\frac{\Delta S_a}{R}\right)\exp\left(-\frac{\Delta H_a}{RT}\right) \qquad (13)$$

Where E_a is the apparent activation corrosion energy, R is the universal gas constant, A is the Arrhenius pre-exponential factor, h is Plank's constant, N is Avogadro's number, ΔS_a is the entropy of activation and ΔH_a is the enthalpy of activation.

Table 5. Temperature influence on the PDP parameters for carbon steel in 1M HCl with and without HCl (1 M) $+10^{-3}$ M of TRD at range temperature 303K-333K.

Inhibitor	Temperature (K)	E_{corr} (mV/SCE)	I_{corr} (mA cm^{-2})	βa (mV dec^{-1})	-βc (mV dec^{-1})	η(%)	θ
	303	-452.1	0.858	113.7	131.2	-	-
Blank	313	-454.1	1.962	109.6	152.3	-	-
	323	-441.9	4.255	147.3	170.4	-	-
	333	-450.1	7.247	151.2	162.9	-	-
	303	-438.8	0.110	71.4	161.6	87	0.87
TRD	313	-429.1	0.434	89.9	209.0	77.8	0.778
	323	-433.3	1.085	107.5	228.3	74.5	0.745
	333	-437.5	2.037	119.9	233.9	71.8	0.718

The values of enthalpy and entropy of activation for carbon steel corrosion in 1.0 M HCl with and without TRD can be evaluated from the slope and intercept of the curve of Ln (I_{corr}/T) versus 1/T, respectively as shown in Fig. 9. It can be

seen in table 6 that the values of enthalpies ΔH_a have a positive signs. This observation can be explain by the endothermic nature of the steel dissolution process and mean that the dissolution of carbon steel is difficult [72]. In the presence of TRD, the increase of ΔS_a reveals that an increase in disordering takes place on going from reactants to the activated complex [73].

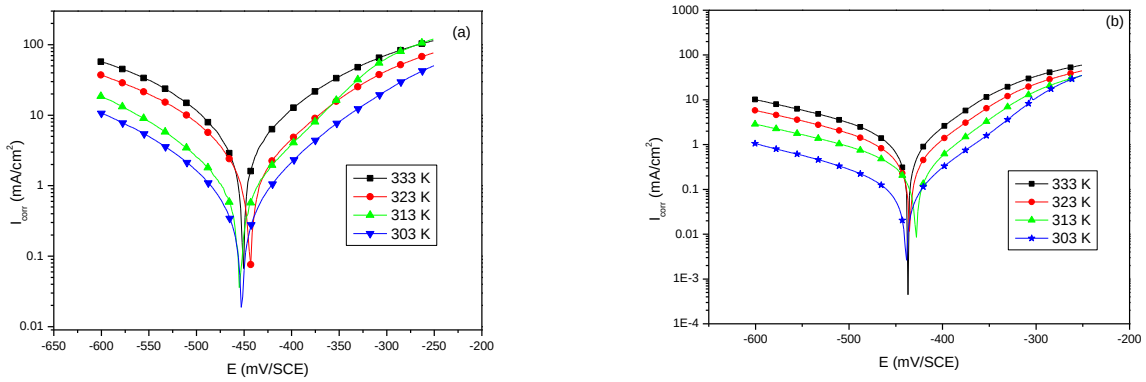

Figure 7. Effect of temperature on the behaviour of carbon steel/1M HCl interface in (a) uninhibited solution, (b) at 10^{-3}M of TRD.

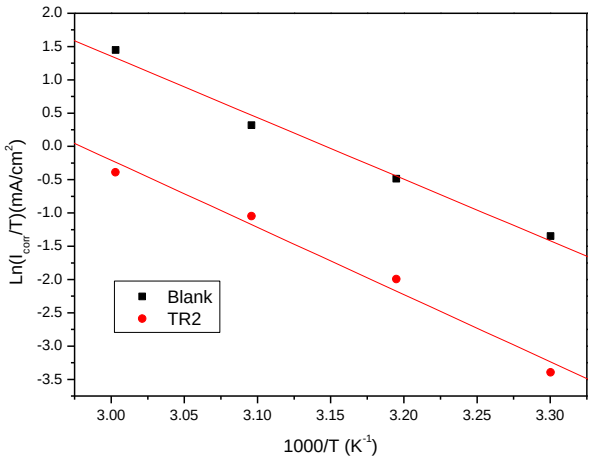

Figure 8. Arrhenius plots for carbon steel in 1M HCl in absence and in presence of 10^{-3}M of TRD.

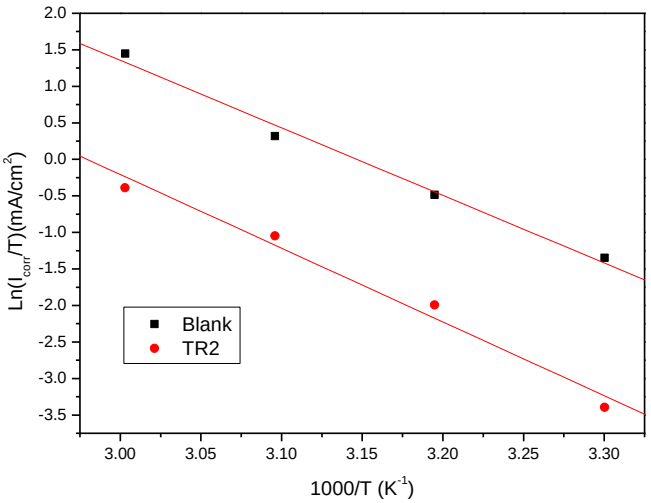

Figure 9. Transition-state plots for carbon steel in 1M HCl in absence and in presence of 10^{-3}M of TRD.

Table 6. Corrosion kinetic parameters for carbon steel in 1M HCl in absence and presence of 10^{-3}M of TRD.

Inhibitor	E_a (KJ.mol^{-1})	ΔH (KJ.mol^{-1})	ΔS (J.mol^{-1}.K^{-1})
Blank	60.3079	76.8798	44.3678
TRD	81.298	83.9374	52.5472

3.6. Theoretical calculations: DFT method

The optimized structure, E_{HOMO} and E_{LUMO} for TRD are shown in Fig. 10. The quantum chemical parameters such as the energy of the highest occupied molecular orbital (E_{HOMO}), the energy of the lowest unoccupied molecular orbital (E_{LUMO}), energy gap (ΔE) and fraction of electron transferred (ΔN) were determined and summarized in Table 8.

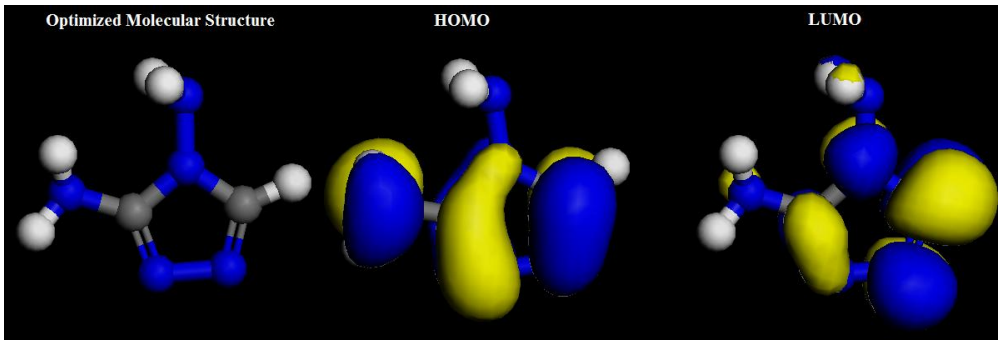

Figure 10. The frontier molecular orbital (*HOMO* and *LUMO*) and optimized molecular structures of the inhibitor.

In Fig. 10, the *HOMO* and *LUMO* orbitals and the electron densities are essentially delocalized over the molecule. These indicate the reactive sites of the inhibitor for interaction between inhibitor molecules and mild steel surface. According to the frontier molecular orbital (*FMO*) theory of chemical reactivity, the formation of a transition state is due to interaction between *HOMO* and *LUMO* of reacting species. The smaller the orbital energy gap (ΔE) between the participating *HOMO* and *LUMO*, the stronger the interactions between two reacting species[74]. It was reported previously that smaller values of ΔE is responsible for higher inhibition efficiency[75,76]. The lower values of the energy gap ΔE will render good inhibition efficiencies since the energy to remove an electron from the last occupied orbital will be minimized[77]. The value of ΔN is used as a gauge of the fraction of electrons transferred from the inhibitor molecule to the iron atom and it is used to predict the mode of electron donation (forward or backward) that results in increase in inhibition efficiency of the inhibitors. According to Lukovits et al.[78] if the value of ΔN is less than 3.6, the inhibition efficiency of the inhibitor increases with increasing electron-donating ability of the inhibitor at the metal surface. In this study, it can be seen from Table 7 that the value of ΔN is less than 3.6, indicating the high tendency of tested compound to react with mild steel, which is in good agreement with the experimental η% values.

Table 7. Calculated quantum chemical parameters of the inhibitor molecule.

Inhibitors	E_{HOMO} (eV)	E_{LUMO} (eV)	ΔE_{gap}	ΔN
TRD	-5.047	0.112	5.159	0.308

3.7. Monte Carlo simulation

Nowadays, molecular dynamics simulation has been extensively used to describe the interactions between the inhibitor and metal surface[79,80]. In our present study, the Monte Carlo simulation calculation was used to find the

lowest energy for the whole system. The outputs and descriptors calculated by the Monte Carlo simulation, such as the total adsorption, adsorption energy, rigid adsorption and deformation energies are presented in Table 8. Fig. 11 represents the most stable low energy configuration for the adsorption of TRD on Fe (1 1 0) surface obtained through the Monte Carlo simulations. Generally, the adsorption energy is defined as the sum of rigid adsorption energy and the deformation energy for the adsorbate component (TRD). Whereas, the rigid adsorption energy is the energy in kcal/mol which is either released or absorbed when the unrelaxed TRD molecules adsorbed on the Fe (1 1 0) surface. The deformation energy is the energy (in kcal/mol) released when the adsorbed adsorbate components are relaxed on the Fe (1 1 0) surface[43,81]. The quantity (dE_{ads}/dN_i) depicted in Table 8 represents the energy of Fe (1 1 0)-adsorbate configurations where one of the adsorbate component has been removed [81,82]. The results depicted in Table 8 show that the TRD associated with high negative values of adsorption energy resulting in the strong interactions between metal and TRD molecules. Which is an indication of the good inhibitive performance of tested compound.

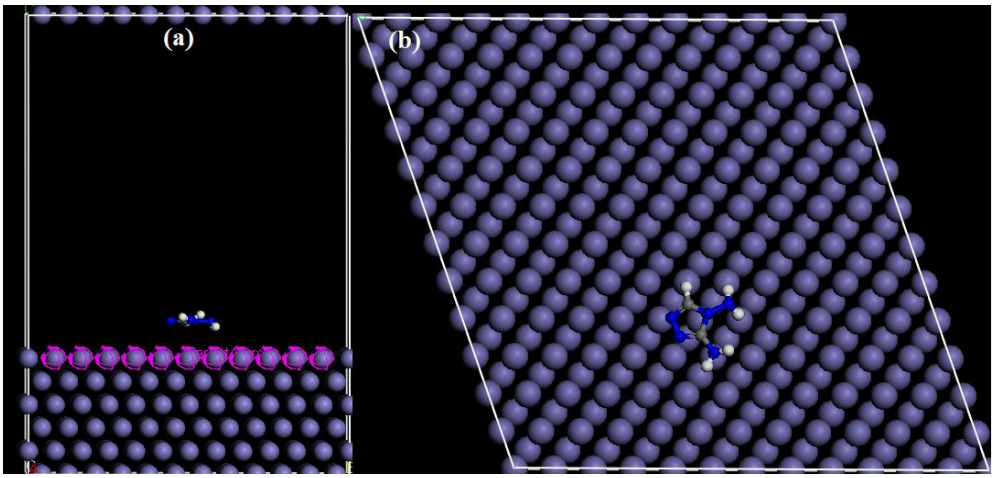

Figure 11. The most stable low energy configuration for the adsorption of the inhibitor on Fe (1 1 0) surface obtained through the Monte Carlo simulation. (a) side view, (b) top view.

Table 8. Outputs and descriptors calculated by the Monte Carlo simulation for the lowest adsorption configurations of TRD on Fe (1 1 0) surface (in kcal/mol).

System	Total energy	Adsorption Energy	Rigid adsorption energy	Deformation energy	dEad/dNi inhibitor
Fe (1 1 0)/TRD	-66.70	-72.69	-53.71	-18.98	-72.69

4. Conclusion

In the present report, The 3,4-diamino-1,2,4-triazole shows good inhibition properties for the corrosion of carbon steel in 1M HCl. The inhibition efficiency, η(%) increases with increasing of concentration of the inhibitor, reaching it maximum value at 10^{-3} M of concentration. The corrosion process is inhibited by the adsorption of TRD on steel surface and the adsorption of this inhibitor fits a Langmuir isotherm model at 303 K. The calculated values of ΔG_{ads}^{o} reveal that the adsorption mechanism of TRD on carbon steel surface in 1M HCl solution is mainly physisorption and chemisorption. Based on the Tafel polarization results, TRD can be classified as mixed type inhibitor. The effeciency of this inhibitor is found to decrease proportionally with increasing temperature (303–333 K). The double layer capacitance obtained from EIS measurements decreases with the augmentation of inhibitor concentration, confirming

an adsorption process of the TRD on the carbon steel surface. The potential zero charge (pzc) results showed that the CS surface was positively charged in the presence of the inhibitor studied. Data obtained from quantum chemical calculations were correlated to the inhibitive effect of triazole derivative. Both experimental and theoretical calculations are in excellent agreement.

References

[1] W. Wang, E.J. Peter, R. Zhiyong, Corros. Sci. 57 (2012) 215.

[2] H.M. Abd El-Lateef, *Corros. Sci*. 92 (2015) 104–117.

[3] M. Mousavi, H. Safarizadeh, A. Khosravan, *Corros. Sci*. 65 (2012) 249–258.

[4] K. Zhang, B. Xu, W. Yang, X. Yin, Y. Liu, Y. Chen, *Corros. Sci*. 90 (2015) 284–295.

[5] A.K. Singh, S.K. Shukla, M.A. Quraishi, E.E. Ebenso, *J. Taiwan Inst. Chem. Eng*. 43 (2012) 463–472.

[6] A. Ehsani, M.G. Mahjani, R. Moshrefi, H. Mostaanzadeh, J.S. Shayeh, *RSC Adv* 4 (2014) 20031–20037.

[7] D.O. Isin, N. Karakus, *J. Taiwan Inst. Chem. Eng*. 50 (2015) 306–313.

[8] M. Tourabi, K. Nohair, M. Traisnel, C. Jama, F. Bentiss, *Corros. Sci*. 75 (2013) 123–133.

[9] L.B. Tang, X.M. Li, L. Li, Q. Qu, G.N. Mu, G.H. Liu, *Mat. Chem. Phys*. 94 (2005) 353.

[10] L.B. Tang, X.M. Li, L. Li, G.N. Mu, G.H. Liu, *Mat. Chem. Phys*. 97 (2006) 301.

[11] L.B. Tang, X.M. Li, Y.S. Si, G.N. Mu, G.H. Liu, *Mat. Chem. Phys*. 95 (2006) 29.

[12] X.M. Li, L.B. Tang, L. Lin, G.N. Mu, G.H. Liu, *Corros. Sci*. 48 (2006) 308.

[13] X.M. Li, L.B. Tang, *Mat. Chem. Phys*. 90 (2005) 286.

[14] L.B. Tang, X.M. Li, G.N. Mu, G.H. Liu, L. Li, H.C. Liu, Y.S. Si, *J. Mat. Sci*. 41 (2006) 3063.

[15] L.B. Tang, X.M. Li, G.N. Mu, L. Li, G.H. Liu, *Appl. Surf. Sci*., in press.

[16] F. Bentiss, C. Jama, B. Mernari, H. El Attari, L. El Kadi, M. Lebrini, M. Traisnel, M. Lagrenée, *Corros. Sci*, 51 (2009) 1628–1635

[17] D.M. Gurudatt, K. N. Mohana, H. C. Tandon, *Journal of Molecular Liquids* 211 (2015) 275–287

[18] W.D. Collins, R.E. Weyers, I.L. Al-Qadi, *Corrosion* 49 (1993) 74.

[19] B. Mernari, H. El Attari, M. Traisnel, F. Bentiss, M. Lagrenée, *Corros. Sci*. 40 (1998) 391–399.

[20] F. Bentiss, M. Lagrenée, M. Traisnel, J.C. Hornez, *Corros. Sci*. 41 (1999) 789–803.

[21] F. Bentiss, M. Traisnel, H. Vezin, M. Lagrenée, *Ind. Eng. Chem. Res*. 39 (2000) 3732–3736.

[22] F. Bentiss, M. Traisnel, M. Lagrenée, *Br. Corros. J*. 35 (2000) 315–320.

[23] M.A. Quraishi, D. Jamal, *Mater. Chem. Phys*. 68 (2001) 283–287..

[24] M. Lagrenée, B. Mernari, M. Bouanis, M. Taisnel, F. Bentiss, *Corros. Sci*. 44 (2002) 573–588.

[25] F. Bentiss, M. Lagrenée, B. Elmehdi, B. Mernari, M. Traisnel, *Corrosion* 58 (2002) 399–407.

[26] M.A. Quraishi, H.K. Sharma, *Mater. Chem. Phys*. 78 (2003) 18–21.

[27] L. Wang, *Corros. Sci*. 48 (2006) 608–616.

[28] F. Bentiss, M. Bouanis, B. Mernari, M. Traisnel, H. Vezin, M. Lagrenée, *Appl. Surf. Sci*. 253 (2007) 3696–3704.

[29] M. Lebrini, M. Traisnel, M. Lagrenée, B. Mernari, F. Bentiss, *Corros. Sci*. 50 (2008) 473–479.

[30] F. Bentiss, C. Jama, B. Mernari, H. El Attari, L. El Kadi, M. Lebrini, M. Traisnel, M. Lagrenée, *Corros. Sci*. 51 (2009) 1628–1635.

[31] S. Zhang, Z. Tao, S. Liao, F. Wu, *Corros. Sci*. 52 (2010) 3126–3132.

[32] A.Y. Musa, A.A.H. Kadhum, A.B. Mohamad, M.S. Takriff, *Corros. Sci*. 52 (2010) 3331–3340.

[33] A.Y. Musa, A.B. Mohamad, A.A.H. Kadhum, M.S. Takriff, *Int. J. Electrochem. Sci*. 6 (2011) 2758–2766.

[34] H. Zarrok, A. Zarrouk, B. Hammouti, R. Salghi, C. Jama, F. Bentiss, *Corros. Sci*. 64 (2012) 243–252.

[35] A. Zarrouk, B. Hammouti, S.S. Al-Deyab, R. Salghi, H. Zarrok, C. Jama, F. Bentiss, *Int. J. Electrochem. Sci.* 7 (2012) 5997- 6011.
[36] Materials Studio, Revision 6.0, Accelrys Inc., San Diego, USA, 2013.
[37] B. Delley, *J. Chem. Phys*. 92 (1990) 508–517.
[38] B. Delley, From molecules to solids with the DMol3 approach, *J. Chem. Phys*. 113 (2000) 7756–7764.
[39] V. Sastri, J. Perumareddi, *Corrosion*. 53 (1997) 617–622.
[40] R.G. Pearson, *Inorg. Chem*. 27 (1988) 734–740.
[41] S. Martinez, *Mater. Chem. Phys*. 77 (2003) 97–102.
[42] I. Lukovits, E. Kalman, F. Zucchi, *Corrosion*. 57 (2001) 3–8.
[43] A.R. Eivani, J. Zhou, J. Duszczyk, Comput. *Mater. Sci*. 54 (2012) 370–377.
[44] D.B. Hmamou, R. Salghi, A. Zarrouk, H. Zarrok, R. Touzani, B. Hammouti, A. El Assyry, *J. Environ. Chem. Eng*. 3 (2015) 2031–2041
[45] S. Kaya, B. Tüzün, C. Kaya, I.B. Obot, *J. Taiwan Inst. Chem. Eng*. 58 (2016) 528–535.
[46] S.S. Abd EI-Rehim, M.A.M. Ibrahim, K.F. Khaled, *J. Appl. Electrochem*. 29 (1999) 593.
[47] M. Bouklah, N. Benchat, A. Aouniti, B. Hammouti, M. Benkaddour, M. Lagrenée, H. Vezin, F. Bentiss, *Prog. Org. Coat*. 51 (2004) 118.
[48] R. Solmaz, *Corros. Sci.* 52 (2010) 3321–3330.
[49] A. Ehsani, M.G. Mahjani, M. Nasseri, M. Jafarian, *Anti-Corros. Methods Mater*. 61 (2014) 146–152.
[50] A. Ehsani, M.G. Mahjani, R. Moshrefi, H. Mostaanzadeha, J.S. Shayeh, *RSC Adv*. 4 (2014) 20031–20037.
[51] A. Ehsani, M. Nasrollahzadeh, M.G. Mahjani, R. Moshrefi, H. Mostaanzadeh, *J. Ind. Eng. Chem*. 20 (2014)4363–4370.
[52] A. Popova, M. Christov, *Corros. Sci*. 48 (2006) 3208–3221.
[53] C.H. Hsu, F. Mansfeld, *Corrosion* 57 (2001) 747–748.
[54] D.A. Lopez, S.N. Simison, S.R. deSanchez, *Electrochim. Acta* 48 (2003) 845–854.
[55] B.A. Boukamamp, Solid State Ionics 20 (1980) 31 (b) International Report CT 89/214/128, University of Twente, Eindhoven, the Netherlands (1989).
[56] A. Popova, M. Christov, A. Vasilev, *Corros. Sci*. 49 (2007) 3290–3302.
[57] D.M. Gurudatt, K.N. Mohana, *Ind. Eng. Chem. Res*. 53 (2014) 2092–2105
[58] S. Ghareba, S. Omanovic, *Corros. Sci*. 52 (2010) 2104–2113.
[59] A. Hamdy, N.Sh. El-Gendy, *Egypt. J. Pet*. 22 (2013) 17–25.
[60] A. Popova, M. Christov, *J. Univ. Chem. Technol. Metall*. 43 (2008) 37–47.
[61] C.M. Goulart, A. Esteves-Souza, C.A. Martinez-Huitle, C.J.F. Rodrigues, M.A.M. Maciel, A. Echevarria, *Corros. Sci*. 67 (2013) 281–291.
[62] M.A. Amin, M.M. Ibrahim, *Corros. Sci*. 53 (2011) 873–885.
[63] M.A. Amin, M.A. Ahmed, H.A. Arida, T. Arslan, M. Saraçoglu, F. Kandemirli, *Corros. Sci*. 53 (2011) 540–548.
[64] F. Bentiss, M. Lebrini, M. Lagrenee, *Corros. Sci*. 47 (2005) 2915–2931.
[65] X.M.Wang, H.Y.Yang, F.H.Wang, *Corros. Sci*. 53 (2011) 113-121
[66] L.I. Antropov, E.M. Makushin, V.F. Panasenko, Metal corrosion inhibitors, *Technika, Kiev*, 1981, p, 182.
[67] M. Lebrini, M. Lagrenee, H. Vezin, L. Gengembre, F. Bentiss, *Corros. Sci*. 47 (2005) 485–505.
[68] L. El Ouasif, I. Merimi, H. Zarrok, M. El ghoul, R. Achour, M. Guenbour, H. Oudda, F. El-Hajjaji, B. Hammouti, *J. Mater. Environ. Sci*. 7 (8) (2016) 2718-2730.
[69] M.S. Morad, A.M.K. El-Dean, *Corros. Sci*. 48 (11) (2006) 3398–3412.

[70] M. Lebrini, F. Bentiss, H. Vezin, M. Lagrenée, *Corros. Sci*. 48 (5) (2006) 1279–1291.
[71] J.O'M. Bochris, A.K.N. Reddy, Modern Electrochemistry, vol. 2, Plenum Press, New York, 1977.
[72] B. Hammouti, A. Zarrouk, S.S. Al-Deyab, I. Warad, *Orient. J.Chem*. 27 (1) (2011) 23–31.
[73] S. Martinez, I. Stern, *Appl. Surf. Sci*. 199 (2002) 83–89.
[74] C. Verma, E.E. Ebenso, I. Bahadur, I.B. Obot, M.A. Quraishi, *J. Mol. Liq*. 212 (2015) 209–218.
[75] K.K. Anupama, K. Ramya, A. Joseph, *J. Mol. Liq*. 216 (2016) 146–155.
[76] Y. Sasikumar, A.S. Adekunle, L.O. Olasunkanmi, I. Bahadur, R. Baskar, M.M. Kabanda, I.B. Obot, E.E. Ebenso, *J. Mol. Liq*. 211 (2015) 105–118.
[77] D.K. Singh, S. Kumar, G. Udayabhanu, R.P. John, *J. Mol. Liq.* 216 (2016) 738–746.
[78] I. Lukovits, E. Kálmán, F. Zucchi, *Corrosion.* 57 (2001) 3–8.
[79] M. Shahraki, M. Dehdab, S. Elmi, *J. Taiwan Inst. Chem. Eng*. 62 (2016) 313–321.
[80] Y. Sasikumar, A.S. Adekunle, L.O. Olasunkanmi, I. Bahadur, R. Baskar, M.M. Kabanda, I.B. Obot, E.E. Ebenso, *J. Mol. Liq.* 211 (2015) 105–118.
[81] K.F. Khaled, A. El-Maghraby, Experimental, *Arab. J. Chem*. 7 (2014) 319–326.
[82] I.B. Obot, S. Kaya, C. Kaya, B. Tüzün, *Phys. E Low-Dimens. Syst. Nanostructures*, 80 (2016) 82-90.